CHEST

CrossMark

Prognostic value of radiomic analysis of iodine overlay maps from dual-energy computed tomography in patients with resectable lung cancer

Jooae Choe[1] · Sang Min Lee[1] · Kyung-Hyun Do[1] · Jung Bok Lee[2] · Sang Min Lee[1] · June-Goo Lee[3] · Joon Beom Seo[1]

Abstract

Objectives To investigate whether radiomics on iodine overlay maps from dual-energy computed tomography (DECT) can predict survival outcomes in patients with resectable lung cancer.

Methods Ninety-three lung cancer patients eligible for curative surgery were examined with DECT at the time of diagnosis. The median follow-up was 60.4 months. Radiomic features of the entire primary tumour were extracted from iodine overlay maps generated by DECT. A Cox proportional hazards regression model was used to determine independent predictors of overall survival (OS) and disease-free survival (DFS), respectively.

Results Forty-two patients (45.2%) had disease recurrence and 39 patients (41.9%) died during the follow-up period. The mean DFS was 49.8 months and OS was 55.2 months. Univariate analysis revealed that significant predictors of both OS and DFS were stage and radiomic parameters, including histogram energy, histogram entropy, grey-level co-occurrence matrix (GLCM) angular second moment, GLCM entropy and homogeneity. The multivariate analysis identified stage and entropy as independent risk factors predicting both OS (stage, hazard ratio (HR) = 2.020 [95% CI 1.014–4.026], $p = 0.046$; entropy, HR = 1.543 [95% CI 1.069–2.228], $p = 0.021$) and DFS (stage, HR = 2.132 [95% CI 1.060–4.287], $p = 0.034$; entropy, HR = 1.497 [95% CI 1.031–2.173], $p = 0.034$). The C-index showed that adding entropy improved prediction of OS compared to stage only (0.720 and 0.667, respectively; $p = 0.048$).

Conclusions Radiomic features extracted from iodine overlay map reflecting heterogeneity of tumour perfusion can add prognostic information for patients with resectable lung cancer.

Key Points
• *Radiomic feature (histogram entropy) from DECT iodine overlay maps was an independent risk factor predicting both overall survival and disease-free survival.*
• *Adding histogram entropy to clinical stage improved prediction of overall survival compared to stage only (0.720 and 0.667, respectively; p = 0.048).*
• *DECT can be a good option for comprehensive pre-operative evaluation in cases of resectable lung cancer.*

Keywords Lung neoplasms · Prognosis · Multidetector computed tomography · Diagnostic imaging

✉ Sang Min Lee
sangmin.lee.md@gmail.com

[1] Department of Radiology and Research Institute of Radiology, University of Ulsan College of Medicine, Asan Medical Center, 88 Olympic-ro 43 Gil, Songpa-gu, Seoul 138-736, Korea

[2] Department of Medical Statistics, Asan Medical Center, University of Ulsan College of Medicine, Seoul, Korea

[3] Department of Convergence Medicine, University of Ulsan College of Medicine, Asan Medical Center, Seoul, Korea

Abbreviations

ASM	Angular second moment
CT	Computed tomography
DECT	Dual-energy computed tomography
GLCM	Grey level co-occurrence matrix
GRAD	Absolute gradient
HIST	Histogram analysis
ICC	Interclass correlation coefficient.
OS	Overall survival
PET	Positron emission tomography
RL	Run-length encoding

 Springer

ROC   Receiver operating characteristic
SUVmax   Maximal standard uptake values

Introduction

Lung cancer is the leading cause of cancer-related death [1]. At present, surgical resection offers the best opportunity for long-term survival and cure in patients with lung cancer [2]. However, even after curative resection, 30–55% of patients with lung cancer develop recurrence and die of the disease [3]. The prognosis of patients with lung cancer is predicted largely based on pathological stage. Although pathological staging is simple and easy to use, there are limitations to stratifying patients precisely. Patients at the same stage can exhibit wide variations in their incidence of recurrence and survival after curative resection. For guidance of adjuvant therapies, there is a need to find complementary parameters that can help to predict the prognosis more accurately in patients with resectable disease [4].

Radiomics has attracted attention as a promising prognostic tool for the prediction of patient survival [5–7]. Radiomics extracts and uses large numbers of quantitative imaging features, with high-throughput. Recently Aerts et al showed that radiomics has prognostic power by capturing intratumour heterogeneity in lung cancer, and is associated with underlying gene-expression patterns [8]. However, as radiomic approaches are performed using routine CT scans such as non-contrast or contrast-enhanced images, tumour perfusion and angiogenesis, which are known to be prognostic factors [9–11], cannot be assessed properly.

In this context, dual-energy CT (DECT) enables selective visualisation and quantification of iodine enhancement at certain time points during data acquisition, which can provide additional information on tumour perfusion. Because an iodine map portraying the distribution of iodine in the tissue correlates strongly with blood volume and vascular density of a lesion, DECT can be used as an imaging surrogate for the assessment of tumour angiogenesis [12–14]. Kim et al demonstrated that DECT is practically useful for evaluating the net iodine enhancement of tumours and for evaluating tumour responses to anti-angiogenic treatment, which are reflected by perfusion decreases [13]. Furthermore, according to Bae et al's study, quantitative radiomic values derived from DECT, including uniformity and 97.5th percentile attenuation, showed potential for prediction of pathological invasiveness and prognosis in adenocarcinoma of the lung [14].

We hypothesised that radiomics based on the iodine overlay map could provide additional prognostic information for better stratification of resectable lung cancer. Thus, we performed this study to investigate whether radiomics on iodine overlay maps from DECT can predict survival outcome in patients with resectable lung cancer.

Materials and methods

Study population

Our institutional review board approved this retrospective cohort study, and informed consent was waived. Retrospective review of a database at our institution identified 131 consecutive patients who underwent DECT scans for staging workups of lung cancer at the time of diagnosis, from October 2010 to December 2012. As our study targeted patients with resectable lung cancer, 38 out of 131 patients were excluded from the study for the following reasons: 14 patients had ground-glass nodules, nine patients had stage IV disease (pleural seeding, n = 6; bone and dural metastasis, n = 1; lung metastasis, n = 1; and lung and adrenal metastasis, n =1), 11 patients underwent stereotactic body radiation therapy rather than surgery, two patients were lost to follow-up before treatment, and two patients had double primary cancers that could have affected overall survival (Fig. 1).

A total of 93 patients were finally included in the study (M:F = 66:27, mean age 64.7 ± 9.0 years, range 37–84). In each patient, the primary tumour was visible on the staging CT, with distinguishable tumour margin and histopathological type of tumour, and pathological staging was confirmed through surgery (Table 1).
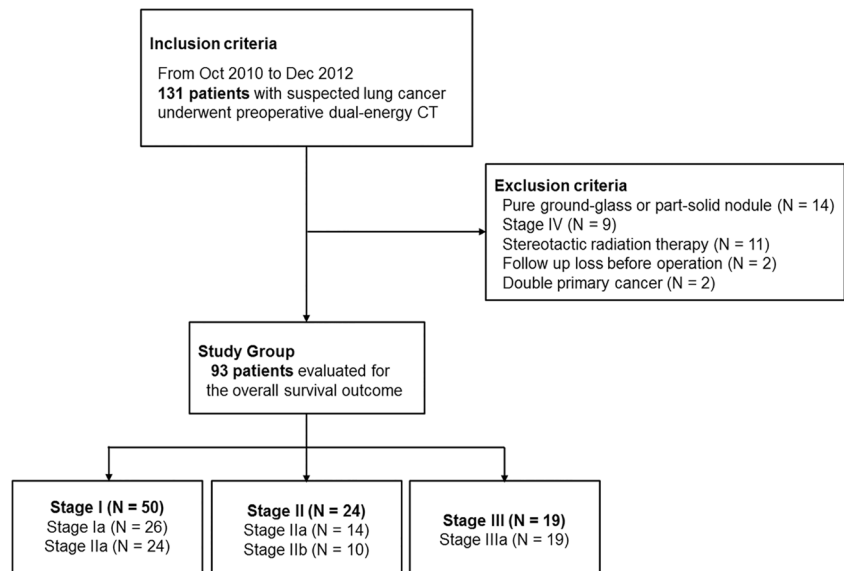
The overall tumour stage of each patient was derived from pathological staging (local-regional) confirmed by surgery, CT and positron emission tomography (PET)/CT, based on the 7th lung cancer TNM classification and staging system of the American Joint Committee on Cancer [15]. In addition to pre-operative CT imaging, maximal standard uptake values (SUVmax) from PET were also collected for the patients for whom it was available (n = 84).

The primary outcomes were disease-free survival (DFS) and overall survival (OS). DFS was defined as the time from the date of surgery until either the date of relapse (event), which refers to local tumour recurrence or distant metastasis, or death, or until the date that the patient was last known to be free of relapse (censored). OS was calculated from the date of surgery until either death from any cause (event) or until the date that the patient was last known to be alive (censored). The survival state of the patients and the date of death were obtained from the Korean national demographic database. The median follow-up was 60.4 months (range 0.7–76.5).

Imaging acquisition – dual-energy perfusion computed tomography

The initial CT scans were obtained within 6 weeks prior to the surgery (interval between perfusion CT and operation: median 12 days, range 0–42). All patients underwent CT examination using a CT system (SOMATOM Definition; Siemens Healthcare, Forchheim, Germany) in the dual-energy mode

Fig. 1 Schematic flow chart of patient inclusion criteria

Inclusion criteria
From Oct 2010 to Dec 2012
131 patients with suspected lung cancer underwent preoperative dual-energy CT

Exclusion criteria
Pure ground-glass or part-solid nodule (N = 14)
Stage IV (N = 9)
Stereotactic radiation therapy (N = 11)
Follow up loss before operation (N = 2)
Double primary cancer (N = 2)

Study Group
93 patients evaluated for the overall survival outcome

Stage I (N = 50)
Stage Ia (N = 26)
Stage IIa (N = 24)

Stage II (N = 24)
Stage IIa (N = 14)
Stage IIb (N = 10)

Stage III (N = 19)
Stage IIIa (N = 19)

(80 and 140 kV). Two sets of spiral CT data were acquired with a collimation of 14 x 1.2 mm, a pitch of 0.5 and a rotation time of 0.33 s. The tube current for the 80 kV level was adjusted to be four times greater than that for the 140 kV level. A total of 125 ml of iodinated contrast agent (Ultravist, 370 mgI/ml; Schering) was injected intravenously using a dual-head power injector at a rate of 2.5 ml/s, followed by a saline chaser of 30 ml at the same injection rate. The scan delay was fixed at 40 s. Images were reconstructed using a medium-soft convolution kernel (D30), with a 1.5 mm slice thickness and a 0.7 mm increment. Three sets of weighted average images, iodine distribution images and overlay images of the weighted images were generated on a commercially available workstation with the pulmonary blood volume application of Syngo Dual Energy (Siemens Healthcare), as described by Chae et al [16, 17]. We used these iodine distribution images as the 'iodine overlay map'.

Data post-processing and image reconstruction

The DECT images were retrieved from the institution's archives and loaded by our in-house software (a medical imaging solution for segmentation and radiomic analysis). Tumour segmentation was performed on weighted-average images to delineate tumour borders, and the resulting mask was applied to the iodine overlay maps. Tumours were drawn three-dimensionally using a semi-automated technique, covering as large a portion of the whole tumour as possible by the software, and then minimally corrected by a radiologist who was blinded to the pathological results and clinical outcome. The interobserver reproducibility was analysed for region-of-interest (ROI)–based texture feature extraction by two experienced radiologists (L.S.M. and J.C.; readers 1 and 2, with 6 and 2 years of experience in chest CT, respectively). Further analyses were performed using the measurements of the first reader.

Histogram- and gradient-based features, along with run-length encoding (RL), absolute gradient (GRAD), moment [18] and grey-level co-occurrence matrix (GLCM)-based features were obtained from a quantitative CT analysis of the automatically derived ROI. Histogram analysis (HIST) was performed for assessment of mean attenuation, skewness (skewness of pixel distribution), kurtosis (magnitude of pixel

Table 1 Patient characteristics

Characteristic	
Age (y)	64.7 ± 9.1
Sex	
Male	66 (71.0)
Female	27 (29.0)
Smoking history	
Current/former smoker	64 (68.8)
Never-smoker	29 (31.2)
Histopathological type	
Squamous cell carcinoma	30 (32.3)
Adenocarcinoma	55 (59.1)
Others	8 (8.6)
Stage	
I	50 (53.8)
II	24 (25.8)
III	19 (20.3)
Median follow-up, months (range)	60.4 (0.7–76.5)
Disease recurrence	42 (45.2)
Deaths	39 (41.9)

Data are presented as mean ± standard deviation or n (%), unless indicated otherwise

distribution), energy and entropy (irregularity). Texture parameters derived from the GLCM were also calculated, including angular second moment (ASM), contrast, correlation, entropy and homogeneity. The derivation of the GLCM of an image was based on the statistical relationships of the intensities of nearby pixels [19].

Statistical analysis

All statistical analyses were performed using SPSS (version 21; IBM, Armonk, NY, USA) and the R statistical package, version 3.1.2 [http://www.r-project.org]). For all comparisons, $p < 0.05$ was considered statistically significant.

The associations of continuous and categorical variables with OS and DFS were evaluated using Cox proportional hazards regression models. In univariate analyses, each variable was included in a Cox regression model alone. Multivariate analyses were performed using the backward elimination method, and variables with p-values < 0.05 in the univariate analysis were used as input variables for multivariate analyses. The removal of variables was based on likelihood ratio statistics, with a probability of 0.10.

Using parameter estimates from the multivariate Cox model, we calculated predictive scores. K-adaptive partitioning, a multi-group partitioning algorithm that divides data into K heterogeneous subgroups based on information from a prognostic factor, was then used to determine the cut-off value of the score that could best separate the patients into groups with poor, intermediate and good survival outcomes (as indicated by the best p-value determined using the log-rank test) [20]. Kaplan-Meier survival curves stratified according to the risk groups were generated. The incremental value of the radiomic feature to the traditional staging system was assessed with the C-index, and the area under the receiver operating characteristic (ROC) curve was calculated. The interobserver reproducibility of feature extraction was evaluated using the interclass correlation coefficient (ICC) [21].

Results

Patients

Among the 93 patients, 42 patients (45.2%) had disease recurrence and 39 patients (41.9%) died during the follow-up period. The mean DFS was 49.8 ± 3.7 months and mean OS was 55.2 ± 2.8 months. The cohort included 55 (59.1%) patients with adenocarcinoma, 30 (32.3%) patients with squamous cell carcinoma and eight (8.6%) patients with other histopathological subtypes of tumour, including sarcomatoid carcinoma and adenosquamous carcinoma. For the pathological staging, 26 (28.0%) patients were diagnosed with stage IA, 24 (25.8%)

with IB, 14 (15.1%) with IIA, 10 (10.8%) with IIB and 19 (20.4%) with IIIA.

Survival analysis: Univariate

In the univariate Cox regression analysis, the significant predictors of survival were stage (stage 1 vs. 3) and radiomic parameters, including histogram energy, histogram entropy, GLCM ASM, GLCM entropy and homogeneity for both DFS and OS (Table 2). GLCM contrast (hazard radio (HR) = 1.070, $p = 0.048$) was the only significant predictor for DFS.

SUVmax showed borderline significance as a predictor of survival ($p = 0.057$ for DFS and 0.076 for OS). Stage was also evaluated by regrouping into two new subgroups, stage 1/2A and stage 2B/3. The regrouped stage was a significant predictor of both DFS and OS (HR = 2.793 for DFS and 2.782 for OS).

Survival analysis: Multivariate

The multivariate Cox regression analysis identified the regrouped overall stage and histogram entropy as independent risk factors predicting DFS (regrouped stage, HR = 2.132, $p = 0.034$; entropy, HR = 1.497, $p = 0.034$; Table 3) and OS (regrouped stage, HR = 2.020, $p = 0.046$; entropy, HR = 1.543, $p = 0.021$; Table 4).

For the prediction of DFS, histogram entropy alone had slightly lower diagnostic performance compared to regrouped stage (C-index, 0.631for entropy and 0.671 for regrouped stage) (Table 3). For the prediction of OS, the diagnostic performance of regrouped stage and entropy were similar (C-index, 0.667 for regrouped stage and 0.677 for entropy). ROC analysis showed that adding the radiomic feature produced a better model for prediction of overall survival compared to stage only (0.720 and 0.667, respectively; $p = 0.048$, Table 4). Adding radiomic feature to stage also slightly improved the model performance for DFS prediction but without statistical significance (0.703 and 0.671; $p = 0.090$).

Applying this prediction model, a risk score can be calculated using the following formula.

Prediction of DFS:

$$\text{Risk-score} = 0.757 \times \text{stage } (1 \text{ for stage } 1/2A, 2 \text{ for stage } 2B/3) + 0.404 \times \text{HIST\_entropy}$$

Patients were subsequently classified into a high-risk group (G3; risk-score > 2.99, n = 13), an intermediate-risk group (G2; 1.64 < risk-score ≤ 2.99, n = 65) and a low-risk group (G1; risk-score ≤ 1.64, n = 15).

Prediction of OS:

$$\text{Risk-score} = 0.703 \times \text{stage } (1 \text{ for stage } 1/2A, 2 \text{ for stage } 2B/3) + 0.434 \times \text{HIST\_entropy}$$

Table 2 Univariate analysis of tumour parameters for predicting disease-free survival and overall survival

Parameter	Disease-free survival			Overall survival		
	HR	95% CI	p	HR	95% CI	p
Age	1.018	0.981–1.056	0.355	1.028	0.991–1.067	0.142
Sex (male)	1.366	0.671–2.779	0.390	1.858	0.854–4.044	0.119
Smoking status*	0.961	0.499–1.852	0.961	1.479	0.721–3.036	0.286
Stage (1 vs. 2 vs. 3)	3.652	1.779–7.507	<0.001	2.761	1.288–5.919	0.009
	2.070	0.978–4.383	0.057	1.885	0.881–4.033	0.102
Stage (1,2A vs. 2B,3)	2.793	1.510–5.168	0.001	2.782	1.479–5.234	0.002
SUVmax	1.051	0.999–1.106	0.057	1.045	0.995–1.098	0.076
HIST_mean	1.001	1.000–1.001	0.155	1.001	1.000–1.002	0.109
HIST_SD	1.024	0.992–1.056	0.145	1.017	0.987–1.047	0.274
HIST_skewness	0.991	0.959–1.025	0.611	0.926	0.710–1.207	0.569
HIST_kurtosis	0.99	0.956–1.024	0.552	0.99	0.956–1.024	0.552
HIST_energy	0.053	0.007–0.413	0.005	0.041	0.004–0.382	0.005
HIST_entropy	1.741	1.255–2.416	0.001	1.789	1.27–2.518	0.001
GLCM_ASM	0.078	0.011–0.543	0.010	0.049	0.006–0.424	0.006
GLCM_contrast	1.070	1.000–1.145	0.048	1.048	0.972–1.130	0.219
GLCM_correlation	0.647	0.342–1.224	0.181	0.375	0.135–1.042	0.060
GLCM_entropy	1.767	1.204–2.594	0.004	1.850	1.230–2.781	0.003
GRAD_mean	1.001	0.999–1.003	0.337	1.000	0.999–1.002	0.571
GRAD_SD	1.001	0.999–1.002	0.431	1.000	0.999–1.002	0.698
RL_SRE	81.656	0.127–52657.27	0.182	179.410	0.171–188227.453	0.144
RL_LRE	1.000	0.998–1.003	0.819	1.001	0.998–1.004	0.540
RL_LGRE	0.000	$0.000–16.098 \times 10^{54}$	0.118	0.000	$0.000–2.541 \times 10^{93}$	0.180
RL_HGRE	0.995	0.978–1.012	0.544	0.989	0.972–1.007	0.237
RL_RP	0.117	0.005–2.554	0.173	0.098	0.004–2.695	0.170
Moment_j1	0.981	0.959–1.004	0.100	0.983	0.960–1.007	0.156
Homogeneity	0.018	0.001–0.575	0.023	0.011	0.000–0.433	0.016

HR hazard ratio, *SUVmax* maximum standardised uptake value, *HIST* histogram, *SD* standard deviation, *GLCM* grey-level co-occurrence matrix, *ASM* angular second moment, *RL* run-length, *SRE* short run emphasis, *LRE* long run emphasis, *LGRE* low gray-level run emphasis, *HGRE* high gray-level run emphasis, *RP* run percentage

High-risk group (G3; risk-score > 2.92, n = 15), an intermediate-risk group (G2; 1.78 < risk-score ≤ 2.92, n = 56) and a low-risk group (G1; risk-score ≤ 1.78, n = 22, Fig. 2). Kaplan-Meier survival analyses based on the risk-score showed significant differences in survival between the three groups (Fig. 3).

Interobserver agreement for CT radiomic features

There were no statistically significant differences between the measurements of the two readers for any feature. The interobserver ICCs of all metrics calculated on the basis of the two readers' measurements (except run-length and moment-based texture features) were excellent, ranging

Table 3 Multivariate Cox proportional hazards regression analysis for prediction of disease-free survival and its performance

Parameters	Disease-free survival			5-year disease-free survival
	HR	95% CI	p	C-index
Stage (1,2A vs. 2B,3)	2.132	1.060–4.287	0.034	0.671
HIST_entropy	1.497	1.031–2.173	0.034	0.631
Stage + HIST_entropy				0.703

Table 4 Multivariate Cox proportional hazards regression analysis for prediction of overall survival and its performance

Parameters	Overall survival			5-year overall survival
	HR	95% CI	*p*	*C*-index
Stage (1,2A vs. 2B,3)	2.020	1.014–4.026	0.046	0.667
HIST_entropy	1.543	1.069–2.228	0.021	0.677
Stage + HIST_entropy				0.720
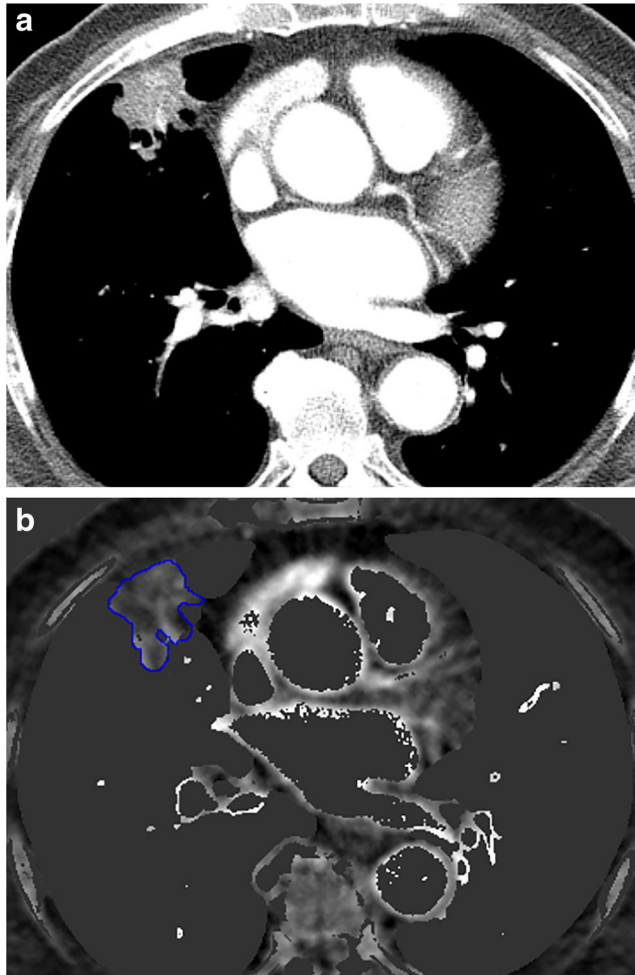
Fig. 2 A 78-year-old man with non-small-cell lung cancer who underwent pre-operative dual-energy perfusion computed tomography (CT). Preoperative CT showed a 4.3 cm irregular enhancing mass in the right middle lobe in contact with the pleura and associated mild pleural thickening (**a**). The same anatomical tumour is shown on the iodine overlay map and the blue line denotes the region of interest (ROI) for radiomic analysis (**b**). Histogram entropy in this patient was 2.41. The patient underwent right middle lobectomy and chest wall invasion was confirmed. The final pathological stage of lung cancer was stage 2B (T3 N0 M0). Regarding the risk-score using regrouped pathological stage and histogram entropy, the patient was grouped into the intermediate-risk group (disease-free survival risk score 2.48, overall survival risk-score 2.45). There was no relapse and the overall survival was 56.9 months

from 0.929 to 0.996 (all *p*-values < 0.0001, Table 5). The run-length-based texture features showed moderate reliability (ICC = 0.653–0.753), and the moment-based feature showed good reliability (ICC = 0.813).

Discussion

This is the first study using radiomic features extracted from a DECT iodine overlay map to predict the prognosis of patients with resectable lung cancer. Our study showed that radiomics feature from DECT iodine overlay map was an independent predictor of survival including both OS and DFS, with an incremental value when incorporated with the staging system.

Table 5 Interclass correlation coefficient for the quantitative histogram- and gradient-based parameters

Measurements	Mean ICC	95% limits of agreement
HIST_mean	0.995	0.993–0.997
HIST_SD	0.996	0.994–0.997
HIST_skewness	0.965	0.947–0.977
HIST_kurtosis	0.929	0.893–0.953
HIST_energy	0.980	0.970–0.987
HIST_entropy	0.987	0.980–0.991
GLCM_ASM	0.975	0.963–0.984
GLCM_contrast	0.992	0.988–0.995
GLCM_correlation	0.995	0.993–0.997
GLCM_entropy	0.987	0.981–0.992
GRAD_mean	0.983	0.974–0.989
GRAD_SD	0.988	0.981–0.992
RL_SRE	0.753	0.628–0.836
RL_LRE	0.653	0.477–0.770
RL_LGRE	0.683	0.522–0.790
RL_HGRE	0.719	0.576–0.814
RL_RP	0.697	0.543–0.799
Moment_j1	0.813	0.718–0.876
Homogeneity	0.985	0.977–990

ICC interclass correlation coefficient, *HIST* histogram, *SD* standard deviation, *GLCM* grey-level co-occurrence matrix, *ASM* angular second moment, *RL* run-length, *SRE* short run emphasis, *LRE* long run emphasis, *LGRE* low gray-level run emphasis, *HGRE* high gray-level run emphasis, *RP* run percentage

The combination of stage and radiomic feature successfully stratified the patients into high-, intermediate- and low-risk groups, with significant differences in 5-year OS and DFS.

In our study, histogram energy, histogram entropy, GLCM ASM, GLCM entropy and homogeneity were consistently significant in the univariate analysis for predicting both OS and DFS. These features reflect the heterogeneity of a tumour, and our results are consistent with those of recent studies that evaluated prognostic radiomic parameters and risk stratification of lung cancer in cross-sectional imaging [22–24]. However, the implications of heterogeneity in an iodine overlay map can be different from those of heterogeneity in non-contrast and contrast-enhanced images. Because the DECT technique allows selective visualisation and quantification of iodine-related attenuation, and thus enables quantification of tumour blood supply more accurately at the time of CT scan than routine enhanced CT [16, 25], heterogeneity on an iodine map may represent heterogeneity of intratumoral perfusion and permeability, which will be different among regions of well-oxygenated tissue, hypoxia or necrosis. Heterogeneity of intratumoral perfusion, especially for necrosis, which is associated with aggressive tumour behaviour and reduced survival, has been recognised in previous studies as a prognostic factor in patients with lung cancer [26–28]. Therefore, based on our results, we believe that radiomic analysis of iodine overlay maps may capture the status of blood supply within a tumour.

Our final prediction model combined histogram entropy and staging (C-index, 0.72 for OS and 0.70 for DFS). The fact that histogram entropy showed significant additional value for prediction of OS demonstrates that radiomic features of iodine overlay maps can provide new information on lung cancer prognosis. For the prediction of DFS, adding histogram entropy to stage also slightly increased the performance but did not show statistical significance, which might result from irregular follow-up intervals exhibited in the patients. The performance of our prediction model incorporating radiomic features was comparable or better than that of previous studies using radiomics (C-index: 0.65–0.72), although there were differences in study population and endpoints for survival [8, 24]. Therefore, we believe that radiomic features derived from iodine overlay maps can be used for survival estimation, and may help to determine the management of patients in terms of patient-tailored treatment. Given that DECT has several advantages in addition to evaluation of lung cancer staging, including better characterisation of tumour using iodine-enhanced images and virtual non-contrast images without additional radiation doses [29], pre-operative/post-operative functional evaluation of surgical candidates [17] and additional prognostic information [14], DECT can be a good option for comprehensive evaluation in cases of resectable lung cancer. However, as we did not compare the performance of radiomic features between routine CT images and DECT-derived iodine
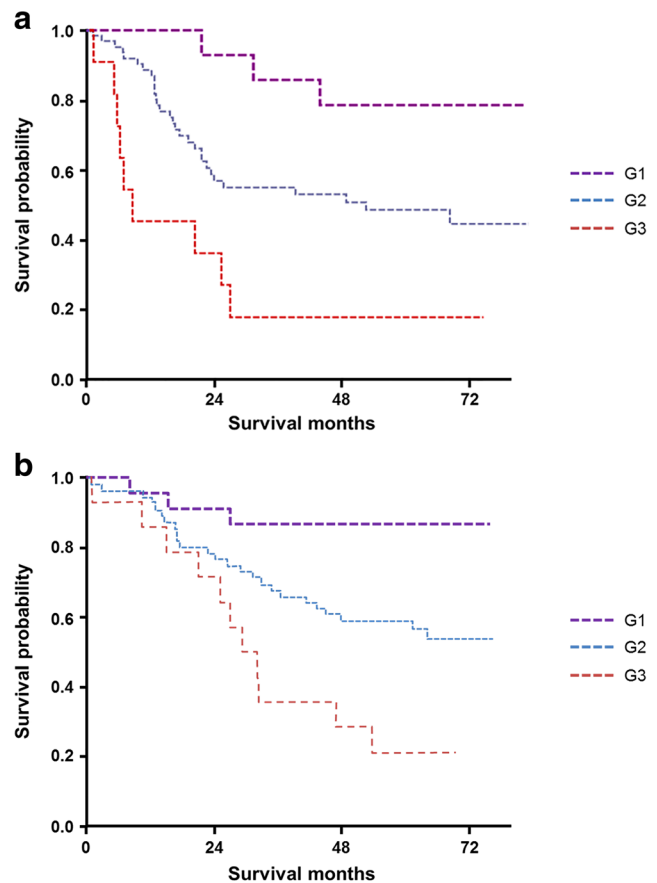

Fig. 3 Prediction model for survival analysis using stage and radiomic features extracted from an iodine overlay map. Kaplan-Meier curves for disease-free survival (**a**) and overall survival (**b**). G1, G2 and G3 are risk groups defined by the prediction model

overlay maps, further studies are needed to verify whether a multiparametric radiomics approach using several CT images (non-contrast, contrast-enhanced and iodine overlay map images) could further improve performance in survival prediction.

The results indicated that histogram- and gradient-based features using a three-dimensional semi-automatically drawn ROI covering the whole tumour on iodine map were all reproducible. Although one of the main challenges of radiomics is tumour segmentation and reproducibility, the interobserver agreement in our study showed an excellent range of ICC. The entropy in particular was a robustly reproducible parameter (ICC = 0.987). In previous lung cancer research, interobserver agreement for texture features ranged from 0.752 to 1.00. The ICC was mostly higher than this in our study; the difference might be caused by a different method of tumour segmentation, using a semiautomatic region-growing volumetric segmentation algorithm with minimal manual correction by a reader. Semiautomatic volumetric segmentation is known to reduce interobserver variability, and significantly improve the robustness of radiomic feature quantification, compared to manual segmentation [30, 31].

Interestingly, SUVmax showed marginal significance for prediction of survival in patients with resectable lung cancer ($p = 0.076$). It is well known that high values of SUVmax are associated with a higher risk of disease recurrence or death in lung cancer patients [32, 33]. However, there is high measurement variability in reported SUV values derived from FDG-PET/CT in clinical practice between different centres, due to different time of FDG injection, start of scanning, instrument performance changes, execution/interpretation of the examination and condition of the patient [34, 35]. The marginal significance of SUVmax in our study might be due to the retrospective nature of the study, and to measurement variance of SUVmax values, which were based on scans acquired and evaluated in several different centres.

Our study had several limitations. First, the study was performed in a single centre using a retrospective design. Also, the study population was relatively small. Therefore, the generalizability of our results may be limited. However, the DECT data were all acquired using the same machine, which is subjected to a robust quantitative analysis. Our study demonstrated the usefulness of radiomic analysis of iodine overlay map and provided evidence for expanding the scope of radiomic approaches. Second, as we used in-house software in our study, a multicentre reproducibility study may be warranted. Finally, an inherent limitation of DECT is that it can only provide a static picture of pulmonary perfusion at a particular time point and iodine enhancement can be influenced by several confounding factors such as age, sex, body weight and cardiac function of the patient despite the same scanning parameters.

In conclusion, radiomic features extracted from iodine overlay map reflecting heterogeneity of tumour perfusion can add prognostic information for patients with resectable lung cancer. Future prospective studies are needed to further explore the potential of this technique to guide individualised post-operative management for these patients.

Compliance with ethical standards

Guarantor The scientific guarantor of this publication is Dr. Joon Beom Seo.

Conflict of interest The authors of this manuscript declare no relationships with any companies whose products or services may be related to the subject matter of the article.

Statistics and biometry One of the authors (Jung Bok Lee, PhD) has significant statistical expertise.

Informed consent Written informed consent was waived by the Institutional Review Board.

Ethical approval Institutional Review Board approval was obtained.

Methodology
• Retrospective
• Prognostic study
• Performed at one institution

References

1. Siegel RL, Miller KD, Jemal A (2017) Cancer statistics, 2017. CA Cancer J Clin 67:7–30
2. Mitsudomi T, Suda K, Yatabe Y (2013) Surgery for NSCLC in the era of personalized medicine. Nat Rev Clin Oncol 10:235–244
3. al-Kattan K, Sepsas E, Fountain SW, Townsend ER (1997) Disease recurrence after resection for stage I lung cancer. Eur J Cardiothorac Surg 12:380–384
4. Uramoto H, Nakanishi R, Nagashima A et al (2010) A randomized phase II trial of adjuvant chemotherapy with bi-weekly carboplatin plus paclitaxel versus carboplatin plus gemcitabine in patients with completely resected non-small cell lung cancer. Anticancer Res 30: 4695–4699
5. Gerlinger M, Rowan AJ, Horswell S et al (2012) Intratumor heterogeneity and branched evolution revealed by multiregion sequencing. N Engl J Med 366:883–892
6. Nitadori J-i, Bograd AJ, Kadota K et al (2013) Impact of micropapillary histologic subtype in selecting limited resection vs lobectomy for lung adenocarcinoma of 2cm or Smaller. J Natl Cancer Inst 105:1212–1220
7. Patnaik SK, Kannisto E, Knudsen S, Yendamuri S (2010) Evaluation of microRNA expression profiles that may predict recurrence of localized stage I non-small cell lung cancer after surgical resection. Cancer Res 70:36–45
8. Aerts HJ, Velazquez ER, Leijenaar RT et al (2014) Decoding tumour phenotype by noninvasive imaging using a quantitative radiomics approach. Nat Commun 5:4006
9. Straume O, Chappuis PO, Salvesen HB et al (2002) Prognostic importance of glomeruloid microvascular proliferation indicates an aggressive angiogenic phenotype in human cancers. Cancer Res 62:6808–6811
10. Maeda R, Ishii G, Ito M et al (2012) Number of circulating endothelial progenitor cells and intratumoral microvessel density in non-small cell lung cancer patients: differences in angiogenic status between adenocarcinoma histologic subtypes. J Thorac Oncol 7: 503–511
11. Zhao YY, Xue C, Jiang W et al (2012) Predictive value of intratumoral microvascular density in patients with advanced non-small cell lung cancer receiving chemotherapy plus bevacizumab. J Thorac Oncol 7:71–75
12. Son JY, Lee HY, Kim JH et al (2016) Quantitative CT analysis of pulmonary ground-glass opacity nodules for distinguishing invasive adenocarcinoma from non-invasive or minimally invasive adenocarcinoma: the added value of using iodine mapping. Eur Radiol 26:43–54
13. Kim YN, Lee HY, Lee KS et al (2012) Dual-Energy CT in Patients Treated with Anti-Angiogenic Agents for Non-Small Cell Lung Cancer: New Method of Monitoring Tumor Response? Korean J Radiol 13:702–710
14. Bae JM, Jeong JY, Lee HY et al (2017) Pathologic stratification of operable lung adenocarcinoma using radiomics features extracted from dual energy CT images. Oncotarget 8:523–535

15. Sobin LH, Gospodarowicz MKCW (2009) UICC International Union Against Cancer. TNM Classification of Malignant Tumours. Lung and pleural tumours. Wiley-Blackwell, Oxford England, pp 138–146

16. Chae EJ, Song J-W, Seo JB, Krauss B, Jang YM, Song K-S (2008) Clinical Utility of Dual-Energy CT in the Evaluation of Solitary Pulmonary Nodules: Initial Experience. Radiology 249:671–681

17. Chae EJ, Kim N, Seo JB et al (2013) Prediction of Postoperative Lung Function in Patients Undergoing Lung Resection: Dual-Energy Perfusion Computed Tomography Versus Perfusion Scintigraphy. Investigative Radiology 48:622–627

18. Wu K, Garnier C, Coatrieux J-L, Shu H (2010) A preliminary study of moment-based texture analysis for medical images. Conf Proc IEEE Eng Med Biol Soc 2010:5581–5584

19. Soh L., C. T (1999) Texture analysis of SAR sea ice imagery using gray level co-occurrence matrices. IEEE Trans Geosci Remote Sens 37:780–795

20. Eo S, Kang HJ, Hong S, Cho HJ (2014) K-Adaptive Partitioning for Survival Data, with an Application to Cancer Staging

21. Portney LG, M.P. W (2000) Foundations of clinical research: applications to practice, 3rd edn. Prentice Hall, New Jersey

22. Yoon SH, Park CM, Park SJ, Yoon JH, Hahn S, Goo JM (2016) Tumor Heterogeneity in Lung Cancer: Assessment with Dynamic Contrast-enhanced MR Imaging. Radiology 280:940–948

23. Hayano K, Kulkarni NM, Duda DG, Heist RS, Sahani DV (2016) Exploration of Imaging Biomarkers for Predicting Survival of Patients With Advanced Non-Small Cell Lung Cancer Treated With Antiangiogenic Chemotherapy. AJR Am J Roentgenol 206: 987–993

24. Huang Y, Liu Z, He L et al (2016) Radiomics Signature: A Potential Biomarker for the Prediction of Disease-Free Survival in Early-Stage (I or II) Non—Small Cell Lung Cancer. Radiology 281: 947–957

25. Johnson TR, Krauss B, Sedlmair M et al (2007) Material differentiation by dual energy CT: initial experience. Eur Radiol 17:1510–1517

26. Swinson DE, Jones JL, Richardson D, Cox G, Edwards JG, O'Byrne KJ (2002) Tumour necrosis is an independent prognostic marker in non-small cell lung cancer: correlation with biological variables. Lung Cancer 37:235–240

27. Park SY, Lee HS, Jang HJ, Lee GK, Chung KY, Zo JI (2011) Tumor necrosis as a prognostic factor for stage IA non-small cell lung cancer. Ann Thorac Surg 91:1668–1673

28. Kilicgun A, Turna A, Sayar A, Solak O, Urer N, Gurses A (2010) Very important histopathological factors in patients with resected non-small cell lung cancer: necrosis and perineural invasion. Thorac Cardiovasc Surg 58:93–97

29. Kang M-J, Park CM, Lee C-H, Goo JM, Lee HJ (2010) Dual-Energy CT: Clinical Applications in Various Pulmonary Diseases. Radiographics 30:685–698

30. Parmar C, Rios Velazquez E, Leijenaar R et al (2014) Robust Radiomics feature quantification using semiautomatic volumetric segmentation. PLoS One 9:e102107

31. Velazquez ER, Parmar C, Jermoumi M et al (2013) Volumetric CT-based segmentation of NSCLC using 3D-Slicer. Sci Rep 3:3529

32. Liu J, Dong M, Sun X, Li W, Xing L, Yu J (2016) Prognostic Value of 18F-FDG PET/CT in Surgical Non-Small Cell Lung Cancer: A Meta-Analysis. PLoS One 11:e0146195

33. Satoh Y, Onishi H, Nambu A, Araki T (2014) Volume-based parameters measured by using FDG PET/CT in patients with stage I NSCLC treated with stereotactic body radiation therapy: prognostic value. Radiology 270:275–281

34. Kumar V, Nath K, Berman CG et al (2013) Variance of Standardised Uptake Values for FDG-PET/CT Greater in Clinical Practice than Under Ideal Study Settings. Clin Nucl Med 38:175–182

35. Nahmias C, Wahl LM (2008) Reproducibility of standardised uptake value measurements determined by 18F-FDG PET in malignant tumors. J Nucl Med 49:1804–1808